



Cite this: *RSC Adv.*, 2018, 8, 26871

# Surface engineering-modulated porous N-doped rod-like molybdenum phosphide catalysts: towards high activity and stability for hydrogen evolution reaction over a wide pH range†

Liyang Chai,<sup>a</sup> Wenyu Yuan,<sup>b</sup>  Xue Cui,<sup>a</sup> Haiying Jiang,<sup>a</sup> Junwang Tang<sup>c</sup> and Xiaohui Guo \*<sup>a</sup>

Electrochemical water splitting is an economic, green and sustainable route to produce hydrogen through the hydrogen evolution reaction (HER). Nowadays, noble metal-free phosphides have been widely used as catalysts in the HER, showing potential applications for both renewable energy production and environmental remediation. Nevertheless, developing surface self-doped MoP electrocatalysts with high HER performances in a wide pH range still remains a challenge. In this work, a novel synthesis strategy was developed to fabricate porous one-dimensional (1D) nitrogen-doped molybdenum phosphide (N-MoP) nanorods. The prepared N-MoP-800 catalyst exhibits a low onset potential of 65 mV and low Tafel slope of 58.66 mV dec<sup>-1</sup> in 0.5 M H<sub>2</sub>SO<sub>4</sub>, which is almost 2 times higher than that of the pristine MoP nanorod anode. Furthermore, the N-MoP materials show long-term durability for 12 h in a wide pH range. The synergistic effects of pyridinic N and N doping in MoP are responsible for the high catalytic activity of N-MoP under acidic conditions, while the N-Mo component plays a key role in enhancing the HER activity of N-MoP. These interesting findings are helpful for the rational design of highly active HER catalysts. More importantly, this study provides a new strategy to synthesize highly active catalysts with low costs for clean energy conversion.

Received 7th May 2018

Accepted 20th July 2018

DOI: 10.1039/c8ra03909g

rsc.li/rsc-advances

## 1. Introduction

The global energy crisis and serious environmental contamination trigger the fast development of renewable, secure and environmentally-friendly energy sources.<sup>1–4</sup> Hydrogen energy, as an efficient energy carrier, has attracted extensive attention due to its outstanding energy density, environmental benignity and reliability.<sup>5,6</sup> The electrocatalytic HER *via* electrolysis of water is the most economical and effective route for the future hydrogen economy.<sup>7</sup> To date, precious Pt-based materials are the most effective catalysts owing to their low overpotential and good stability. However, the excessive cost and low abundance greatly prevent their practical usage.<sup>8–11</sup> Therefore, developing novel non-noble metal catalysts is of great significance for hydrogen production with sufficient efficiency, high stability, and low cost.

Recently, many new types of non-precious metal materials have been investigated as highly active electrocatalyst towards HER, including Co-, Ni-, Fe-, Mo-based transition metal chalcogenides, nitrides, phosphides, carbides, and some multiple compounds.<sup>12–18</sup> Wherein, a kind of ternary pyrite-type CoPS has been fabricated and act as a high-performance Earth-abundant catalyst for electrochemical hydrogen production with lower catalytic overpotential and outstanding long-term operational stability.<sup>19</sup> Among different metal-based compounds, Mo-based catalytic materials, such as MoS<sub>2</sub>,<sup>20,21</sup> Mo<sub>2</sub>C,<sup>22,23</sup> MoN,<sup>24</sup> MoSe<sub>2</sub>,<sup>25</sup> MoB,<sup>26</sup> MoNi<sub>4</sub>,<sup>27</sup> MoP<sub>2</sub>,<sup>28</sup> and MoP,<sup>29–31</sup> which are considered as promising candidates for hydrogen production owing to their low cost and high catalytic activities. Among them, MoP has attracted special attention because of its high electrical conductivity, adjustable morphology, structure and surface architecture. As a result, many progress of MoP-based electrochemical catalysts has been made recently. Li *et al.*<sup>32</sup> demonstrated a MOFs-assisted strategy to develop MoP @ PC with an onset potential of 77 mV and overpotential of 153 mV at 10 mA cm<sup>-2</sup>. In particular, the electrocatalytic performance of transition metal-based materials can be improved by introducing metallic or non-metallic elements. In particular, the electrocatalytic performance of transition metal-based materials can be improved by introducing metallic or non-metallic elements.

<sup>a</sup>Key Lab of Synthetic and Natural Functional Molecule Chemistry of Ministry of Education, College of Chemistry and Materials Science, Northwest University, Xi'an 710069, P. R. China. E-mail: guoxh2009@nwnu.edu.cn; Tel: +86-29-81535031

<sup>b</sup>Science and Technology on Thermostructural Composite Materials Laboratory, Northwestern Polytechnical University, 710072, Xi'an, P. R. China

<sup>c</sup>Department of Chemical Engineering, UCL, Torrington Place, London, WC1E 7JE, UK

† Electronic supplementary information (ESI) available. See DOI: 10.1039/c8ra03909g



Wang *et al.*<sup>33</sup> proposed the N-doped MoP catalyst by a simple temperature-programmed reduction method, which exhibits outstanding HER activity with a small Tafel slope of 54 mV dec<sup>-1</sup> and a good durability in acid condition. Zhang *et al.*<sup>34</sup> proposes an N-doped CoP on carbon cloth as the novel and effective electrocatalyst for HER in acid media, which -42 mV is required to drive a current density of -10 mA cm<sup>-2</sup>. Wang *et al.*<sup>35</sup> successfully synthesized the P/Co-FeS<sub>2</sub> on carbon fiber paper (CFP) and Ti foil *via* solvothermal, sulfurization, and phosphidation processes. It was found that the P/Co-FeS<sub>2</sub>/Ti foil catalyst exhibited higher HER activity with a low overpotential, a small Tafel slope, and high durability in acidic solution. Above research progress indicated that HER performances can be improved by providing much more catalytic active sites through a facile doping process.

Although some great process of HER from MoP has been realized to a certain extent, some key modulating parameters such as defects, edge and/or surface architectures how to affect the electrocatalytic performances of MoP have not been investigated so far. To our knowledge, the rationale modulation of the materials' surface architectures is increasingly important for optimizing the performance of electrocatalytic materials. The catalytic reactions occur mainly on the surface of catalysts, namely, most of the catalytic active sites should be located on the catalysts' surface. For this reason, the surface conditions, including surface compositions, microstructures, defects and/or vacancies, greatly impact the activity of the catalyst, as these parameters determine the surface adsorption and activation abilities of particular reactants.<sup>36,37</sup> Among them, the N-doping in MoP catalyst can obviously influence the surface electronic state and microstructures so as to better modulate HER performances. Recently, although some process of N-doped molybdenum-based electrocatalysts have been obtained for HER applications,<sup>38-40</sup> these reported molybdenum-based (including MoP) materials display HER performances only in acid medium, which certainly limit their practical applications. Therefore, investigating their HER performances in a wide pH range becomes very emergent and necessary.

In this work, we designed and synthesized a novel porous one-dimensional (1D) nitrogen-doped MoP (N-MoP) nanorods through a simple two-step synthetic strategy, which shows high HER catalytic activities over a wide pH range. Besides, the rod-like MoP materials are allowed to possess remarkable long-term electrochemical stability in different conditions. The excellent HER performances were mainly resulted from the modulated surface-active sites derived from N-doping and modulated surface architectures. In a word, the high electrochemical active MoP materials would possess great potential in future energy conversion and utilization.

## 2. Experimental section

### 2.1 Materials

All chemical reagents are analytical degree without further purification treatment.

### 2.2 Synthesis of Mo<sub>3</sub>O<sub>10</sub>/ethylenediamine (EDA) precursor

Herein, the Mo<sub>3</sub>O<sub>10</sub>/EDA nanowires were prepared according to previous literature.<sup>41</sup> Typically, 1.24 g of (NH<sub>4</sub>)<sub>6</sub>Mo<sub>7</sub>O<sub>24</sub>·4H<sub>2</sub>O was dissolved in 15 mL of deionized water, and 0.8 g of EDA was added into the solution. Then, 1 M of HCl was added into above solution dropwise with magnetic stirring at room temperature, until a white precipitate appeared (pH = 4–5). After stirring for 2 h at 50 °C, the Mo<sub>3</sub>O<sub>10</sub>/EDA nanowire was obtained after washing with water and ethanol for several times, and dried at 60 °C for 12 h (Fig. S1a†).

### 2.3 Synthesis of rod-like N-MoP

The one-dimensional N-MoP structures were obtained by controlling the thermal reduction temperature of Mo<sub>3</sub>O<sub>10</sub>/EDA nanowires. To obtain N-MoP-800, 65 mg Mo<sub>3</sub>O<sub>10</sub>/EDA and 100 mg (NH<sub>4</sub>)<sub>2</sub>HPO<sub>4</sub> (molar ratios of Mo/P = 1 : 2) were placed on opposite ends with (NH<sub>4</sub>)<sub>2</sub>HPO<sub>4</sub> at the upstream side of the porcelain boat, and leave it sealed. The boat was heated in a pipe furnace at 800 °C under Ar/H<sub>2</sub> (10%) for 120 min at a heating rate of 5 °C min<sup>-1</sup>. After naturally cooled down to room temperature, the products could be collected for further measurements. Two different temperatures, 750 °C and 850 °C, are chosen to investigate the effect of the thermal reduction temperature. The obtained materials were denoted as N-MoP-750 and N-MoP-850, respectively. The diagram of the preparation process was described in Fig. 1a.

### 2.4 Synthesis of MoP

First, the MoO<sub>3</sub> product was obtained *via* calcination of Mo<sub>3</sub>O<sub>10</sub>/EDA precursor in air atmosphere at 500 °C for 5 h with a heating rate of 5 °C min<sup>-1</sup>. And then, the MoP was synthesized with the same molar ratios of the precursors (Mo/P = 1 : 2) at 800 °C under Ar/H<sub>2</sub> (10%) for 120 min with a heating rate of 5 °C min<sup>-1</sup>.

### 2.5 Characterization

The phase composition and crystallization of the products were recorded using a diffractometer (XRD, Bruker AXS-D8) with Cu K $\alpha$  radiation at a scanning step of 0.03° s<sup>-1</sup> over the 2 $\theta$  range from 10° to 80°. The morphologies of the samples were observed by field emission scanning electron microscopy (FE-SEM, SU-8010, Japan), while the information on lattice and fringe were investigated by high-resolution transmission electron microscopy (HRTEM, FEI Tecnai G2 F20). X-ray photoelectron spectroscopy (XPS, PHI 5000 VersaProbe II XPS) was used to analyze the composition and valence states (a Monochromated Al K $\alpha$  X-ray source, 1486.6 eV).

### 2.6 Electrochemical measurements

The HER activity was studied by a conventional three-electrode method on a Princeton Applied Research Studio P4000 electrochemical workstation (AMETEK Scientific Instruments) at room temperature. A Pt foil, Ag/AgCl (3.0 M KCl) were used as the counter and reference electrodes, respectively. A glass carbon electrode (GCE: diameter = 3 mm) fabricated by drop-



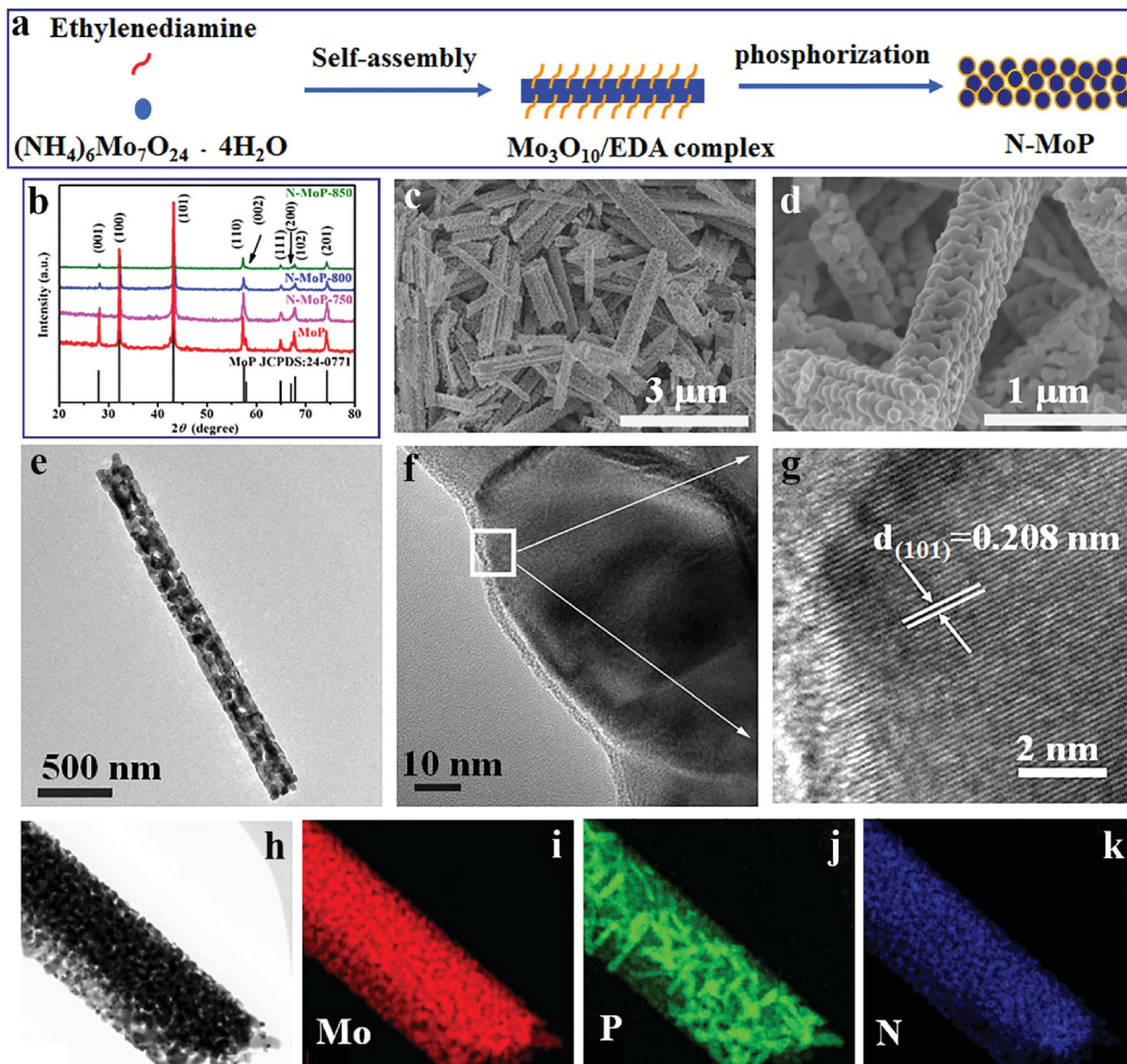


**Fig. 1** (a) Schematic illustration of the formation process of N-MoP; (b) XRD patterns of MoP, N-MoP-750, N-MoP-800 and N-MoP-850; (c and d) FESEM images of N-MoP-800 with different resolutions; (e and f) TEM images and (g) HRTEM image of a part of N-MoP-800 in (f); (h–k) elemental mapping of Mo, P, N of N-MoP-800.

casting the catalyst ink was used as the working electrode. 5 mg of catalyst and 100  $\mu\text{L}$  of 5 wt% Nafion solution were dispersed in 900  $\mu\text{L}$  ethanol by at least 30 min sonication, forming a homogeneous ink. Then 4.3  $\mu\text{L}$  of the catalyst ink (containing 21.5  $\mu\text{g}$  of catalyst) was covered on the GCE (loading amount  $\sim 0.3 \text{ mg cm}^{-2}$ ) with a micropipette and dried naturally in air for test. In all measurements, the  $\text{Ag}/\text{AgCl}$  reference electrode was calibrated with respect to a reversible hydrogen electrode (RHE) by adding a value of  $(0.21 + 0.059 \text{ pH}) \text{ V}$ , and all the potentials reported in our work were *vs.* RHE. Linear sweep voltammetry (LSV) were conducted in 0.5 M  $\text{H}_2\text{SO}_4$  ( $\text{pH} = 0.3$ ), 1 M  $\text{KOH}$  ( $\text{pH} = 14$ ) and 1 M PBS ( $\text{pH} = 7$ ) at a scan rate of  $5 \text{ mV s}^{-1}$ . Electrochemical impedance spectroscopy (EIS) analysis was adopted to provide further insight into the electrical conductivity of

electrocatalysts in the frequency range of  $10^5$  to 0.1 Hz under the amplitude of 10 mV.

$$\text{ECSA} = \frac{C}{40 \mu\text{F cm}^{-2} \text{ per cm}^{-2}} \quad (1)$$

The electrochemical active surface area (ECSA) can be estimated using the capacitance ( $C$ ). The following formula was used to calculate ECSA.<sup>42</sup> To calculate the  $C$  values, cyclic voltammetry (CV) curves were measured under different scan rates that from 10 to 100  $\text{mV s}^{-1}$  in the potential range of 0.1–0.3 V (*vs.* RHE). The durability test was carried out at a static overpotential at a cathodic current density of  $10 \text{ mA cm}^{-2}$  for 12 h.





### 3. Results and discussion

Fig. 1b shows the XRD pattern of the as-prepared sample when the ratio of Mo to P is 1 : 2. The prepared sample can be assigned to pure phase MoP (JCPDS no. 24-0771), which displays well-resolved diffraction peaks at  $2\theta = 27.9^\circ$ ,  $32.2^\circ$ ,  $43.1^\circ$ ,  $57.4^\circ$ ,  $64.9^\circ$ ,  $67.8^\circ$  and  $74.3^\circ$ , corresponding to the (001), (100), (101), (110), (111), (102) and (201) planes, respectively.<sup>43</sup> The XRD patterns display sharp peaks and no impurity peaks can be detected, indicating good crystallization of MoP.

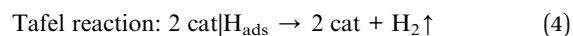
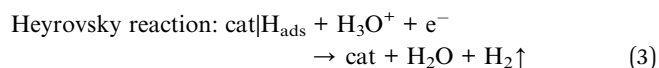
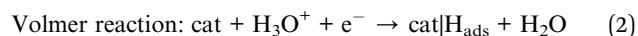
The FESEM images (Fig. 1c and d) show that the N-MoP-800 displays well-defined one-dimensional nanorods structure, meanwhile many bulges and hollows form a porous-like structure on their surfaces. The average diameters and lengths of those nanorods are about 350 nm and 3.2  $\mu\text{m}$ , respectively. A closer observation of N-MoP-800 is provided by TEM and HRTEM testing, as shown in Fig. 1e–g. The nanorods containing numerous nanoparticles can be clearly observed in Fig. 1e. The average diameter of MoP nanoparticles is about 60 nm, as shown in Fig. 1f; it was found that there are obvious humps on the surface of MoP, as shown in Fig. 1d. The HRTEM image in Fig. 1g shows the lattice fringes with a  $d$ -spacing of 0.208 nm, which is assigned to (101) plane of MoP and consistent with the XRD result. The elemental mapping images (Fig. 1h–k) indicate that Mo, P and N elements are uniformly distributed in N-MoP-800 sample. It was noted that the reaction temperature is an important parameter that can influence the morphology and/or microstructure of N-MoP catalyst. The results found that N-MoP-750 and N-MoP-850 display similar rod-like morphology with N-MoP-800, but N-MoP-750 exhibits smaller humps, while N-MoP-850 exhibits nearly the same humps on their surfaces with N-MoP-800, details are shown in Fig. S1–S4.† And the HRTEM images in Fig. S2c and 2f† also show the lattice fringes with a  $d$ -spacing of 0.213 nm and 0.211 nm for N-MoP-750 and N-MoP-850, respectively. Therefore, all the above characterization results demonstrate that the N-MoP materials were successfully prepared by a simple two-step synthetic strategy.

To evaluate the surface elements and their valence states of N-MoP, XPS was carried out. The XPS survey spectrum of the N-MoP-800 sample is shown in Fig. 2a. The existence of Mo, P and N elements can be clearly observed, which is consistent with the elemental mapping results in Fig. 1h–k. Fig. 2b–d show high resolution XPS profiles of Mo 3d, P 2p and N 1s of the as-synthesized N-MoP-800 samples. As shown in Fig. 2b, the peaks at 231.97 eV/228.30 eV ( $3d_{3/2}/3d_{5/2}$ ) generally can be assigned to Mo–P bond, which agrees well with the previous reports.<sup>44,45</sup> In addition, the peaks at 235.84 eV/233.11 eV ( $\text{Mo}^{6+} 3d_{3/2}/3d_{5/2}$ ) and 232.53 eV/228.70 eV ( $\text{Mo}^{4+} 3d_{3/2}/3d_{5/2}$ ) can be assigned to high oxidation state of Mo ( $\text{MoO}_3$  and  $\text{MoO}_2$ ), which is caused by the surface oxidation during the passivation process.<sup>46,47</sup> This passivation process is necessary to prevent the pyrophoric oxidation of MoP when it was exposed in air.<sup>48,49</sup> Moreover, the XPS spectrum of P 2p displays the peaks at a high binding energy of 134.60 eV/133.83 eV due to the presence of surface  $\text{PO}_4^{3-}$  or  $\text{P}_2\text{O}_5$ .<sup>50</sup> Meanwhile, two peaks at 130.62 eV and 129.78 eV, which are attributed to the low valence P in MoP

(Fig. 2c).<sup>32,46</sup> The N 1s XPS spectrum (Fig. 2d) reveals that the existence of the pyridinic N (397.68 eV), pyrrolic N (399.03 eV) and graphitic N (401.78 eV); in addition, the peak at 394.2 eV can be assigned to N-Mo bond.<sup>34</sup> Similar XPS results for N-MoP-750 and N-MoP-850 can be obtained, as shown in Fig. S5 and S6.†

The electrocatalytic activities of the as-synthesized catalysts for the HER were evaluated in a wide pH range. For comparison, commercial 20 wt% Pt/C was also studied under identical conditions. A pure MoP without N doping which was prepared *via* the calcination of  $\text{Mo}_3\text{O}_{10}/\text{EDA}$  precursor in air atmosphere under 500  $^\circ\text{C}$  and a following phosphatization process at 800  $^\circ\text{C}$  under  $\text{Ar}/\text{H}_2$  atmosphere, was used to show the effects of N doping. No N component was observed from the XPS spectra and EDS results, suggesting the successful synthesis of pure MoP without N doping (Fig. S7†). It was proved that MoP without nitrogen doping was successfully prepared by XPS and EDS (Fig. S7†). All tested samples were deposited on a GCE with the same loading amount of 0.3  $\text{mg cm}^{-2}$ . Wherein, the polarization curves of different samples in 0.5 M  $\text{H}_2\text{SO}_4$  were shown in Fig. 3a. It was found that N-MoP-800 exhibited optimal activity with the lowest onset overpotential among these samples of MoP (125 mV), N-MoP-750 (68 mV), N-MoP-800 (65 mV) and N-MoP-850 (95 mV). The overpotential ( $\eta$ ) at  $j = 10 \text{ mA cm}^{-2}$  for the N-MoP-800 is 136 mV, which is lower than the other three samples of MoP (207 mV), N-MoP-750 (148 mV) and N-MoP-850 (163 mV). It was believed that the excellent catalytic activity of N-MoP for HER could be attributed to good conductivity, enhanced active sites and modulated surface architectures after N doping.<sup>51,52</sup>

Tafel slope is commonly used to reveal the reaction mechanism and inherent properties of the catalysts for HER. As we know that, for HER in acidic media, the reaction path is mainly composed of proton adsorption and reduction on the catalyst surface to form  $\text{H}_{\text{ads}}$ , followed by  $\text{H}_2$  formation and desorption.<sup>30,53</sup> These include the Volmer mechanism (electrochemical hydrogen adsorption), the Heyrovsky mechanism (electrochemical hydrogen desorption) and the Tafel mechanism (chemical desorption), detailed as follows:



According to the classical theory on hydrogen evolution mechanism, the Tafel, Volmer or Heyrovsky slopes can be the rate determining step when the Tafel slopes are of about 30, 40 or 120  $\text{mV dec}^{-1}$ , respectively. The Tafel plots for MoP, N-MoP-750, N-MoP-800 and N-MoP-850 are shown in Fig. 3b, their corresponding values are measured to be 77.79, 64.97, 58.66 and 65.32  $\text{mV dec}^{-1}$ , respectively. Therefore, the Tafel slopes for all MoP-based catalysts reveal that the HER proceeds a Volmer–Heyrovsky mechanism, and the Heyrovsky (electrochemical desorption) could become the rate determining step.<sup>44,45,54</sup> A



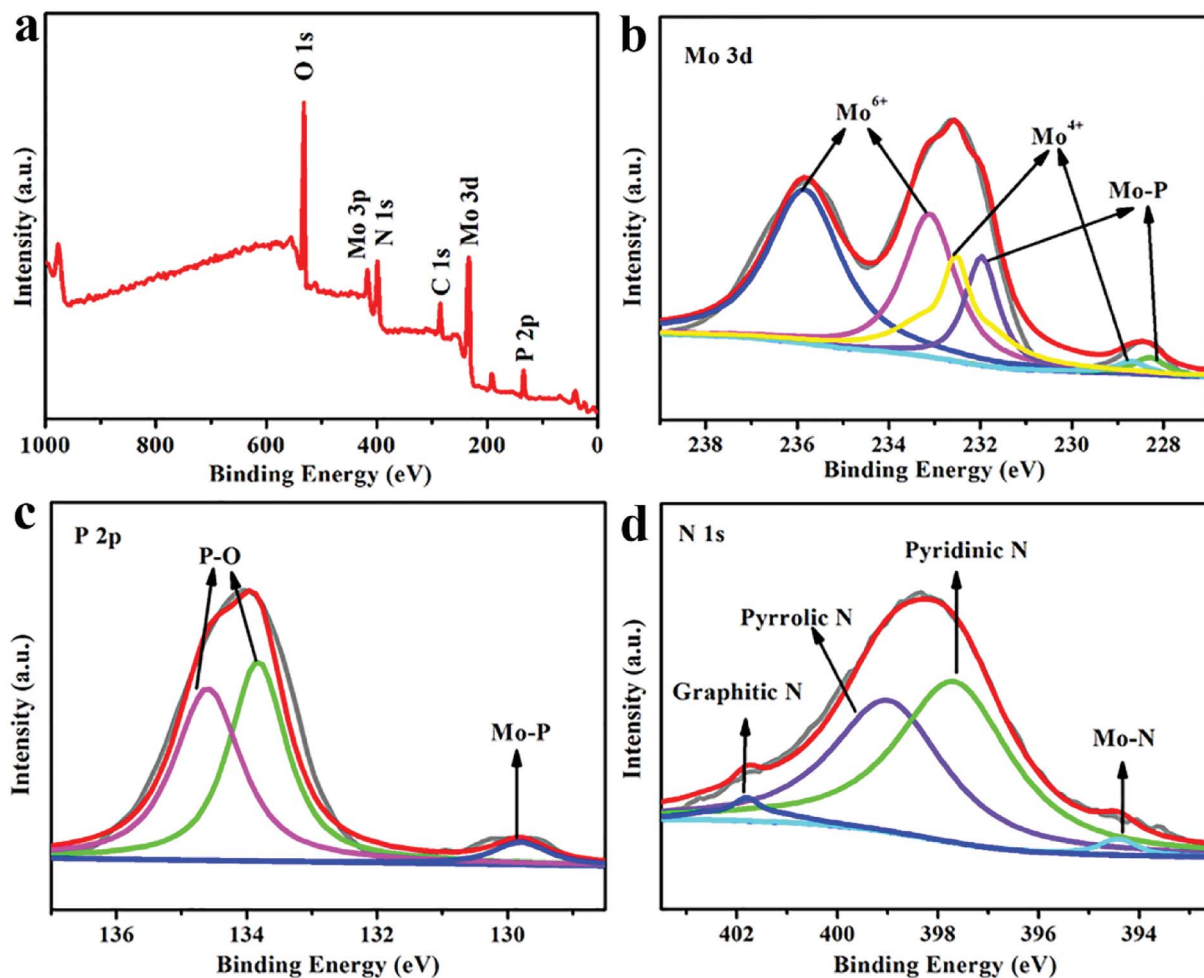


Fig. 2 (a) Wide-scan survey XPS spectrum of N-MoP-800. (b–d) High-resolution XPS signals of (b) Mo 3d, (c) P 2p, and (d) N 1s of N-MoP-800.

smaller Tafel slope would lead to a remarkably higher HER rate with a low overpotential.

The enhancement in catalytic performance of N-MoP-800 can be ascribed to the three main factors: (i) nitrogen doping could generate more active sites and accelerate electron transfer; (ii) the humps and edges on the surface of the N-MoP-800 favor the exposure of more active sites for HER;<sup>38,40</sup> (iii) The

pyridinic N components provide more active sites for HER, further enhanced the activity. According to previous studies, the pyridinic N components can service as the active sites for catalytic reaction.<sup>42,55–57</sup> To show the role of pyridinic N components, the ratios of pyridinic N components in these samples (the content of pyridinic N components/the content of all N-contained groups) were calculated. The N-MoP-800 has

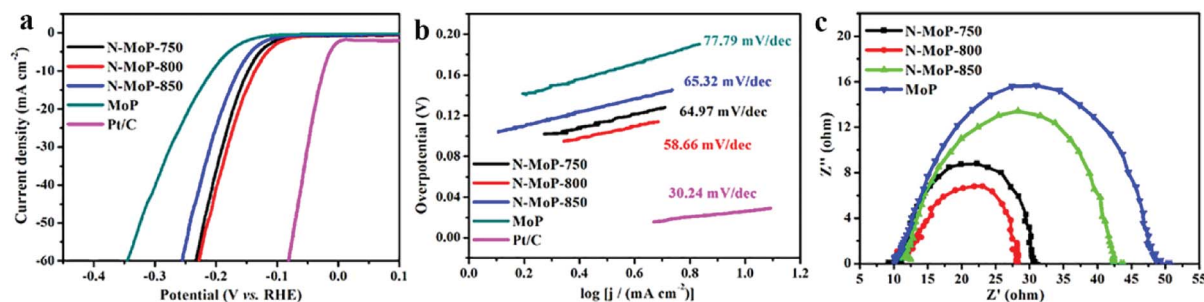


Fig. 3 HER performance of the as-prepared materials in 0.5 M  $\text{H}_2\text{SO}_4$ , (a) polarization curves; (b) Tafel plots for MoP, N-MoP-750, N-MoP-800, N-MoP-850 and Pt/C; (c) Nyquist plots of electrochemical impedance spectra (EIS) of MoP, N-MoP-750, N-MoP-800 and N-MoP-850 recorded at a voltage of  $-172$  mV vs. RHE.



higher proportion pyridinic N components (52.18%) than N-MoP-750 (23.07%) and N-MoP-850 (43.37%), which can provide more active sites, and therefore enhance catalytic activity of N-MoP for HER. Moreover, N-MoP-800 possess larger amount of humps on the surface compared with N-MoP-750 and N-MoP-850, these obvious humps would contribute high active area that can effectively improve electron transfer and provide desirable active sites for pyridinic N components. As a result, the N-MoP-800 displays optimal HER performances among these samples.

In order to elucidate these reasons, further insight into the electrical conductivity of catalysts by ECSA and EIS analysis, so the double-layer capacitor ( $C_{dl}$ ) were investigated. As shown in Fig. 3c, the N-MoP-800 has the smallest value of charge transfer resistance (29  $\Omega$ ), which indicates that N-MoP-800 has faster electron transfer rate compared to that of MoP (52  $\Omega$ ), N-MoP-750 (32  $\Omega$ ) and N-MoP-850 (43  $\Omega$ ). The ECSA of N-MoP-800 was investigated using the  $C_{dl}$ . The results are shown in Fig. 4, the N-MoP-800 has a much higher  $C_{dl}$  (3.72  $\text{mF cm}^{-2}$ ) and ECSA (93.00  $\text{cm}^2$ ), whereas N-MoP-750 has a relative smaller  $C_{dl}$  (2.63  $\text{mF cm}^{-2}$ ) and ECSA (65.75  $\text{cm}^2$ ), N-MoP-850 has the smallest  $C_{dl}$  (2.12  $\text{mF cm}^{-2}$ ) and ECSA (53.00  $\text{cm}^2$ ). Herein, the high ECSA of N-MoP-800 is mainly resulted from the large amounts of humps on the surface. These results fully

demonstrate that the surface engineering-modulated microstructure (*ca.*, doping and humps) has dramatic effect on enhancing the HER activity of MoP.

The long-term electrochemical durability is also a critical parameter for HER catalyst. Fig. 5a shows that the polarization curve of N-MoP-800 do not change after 1000 CV cycles at a scan rate of 50  $\text{mV s}^{-1}$ . Furthermore, the stability of this catalyst was also evaluated by electrolysis at a constant overpotential of 140 mV, and we also found that the current density only undergoes a slight decrease after 12 h testing (Fig. 5b). This is probably due to the specific 1D aggregate structure and rich N-doping on the N-MoP surface.

The catalytic activity of N-MoP was further conducted in 1 M KOH. Generally, the electrocatalytic HER activity in alkaline media requires more energy to generate  $\text{H}^+$ , which leads to the phenomenon that many catalysts with high activity in acid solution suffer from large activity decay in alkaline solution. It was noted that, the onset potential of MoP, N-MoP-800 and N-MoP-850 are about 157 mV, 70 mV and 84 mV, respectively. And the current density can approach 10  $\text{mA cm}^{-2}$  at an overpotential of 293 mV, 157 mV and 156 mV for MoP, N-MoP-800 and N-MoP-850, respectively. N-MoP-750, exhibits a lower onset potential of 68 mV, and achieves a current density of 10  $\text{mA cm}^{-2}$  at an overpotential of 145 mV (Fig. 6a). The above

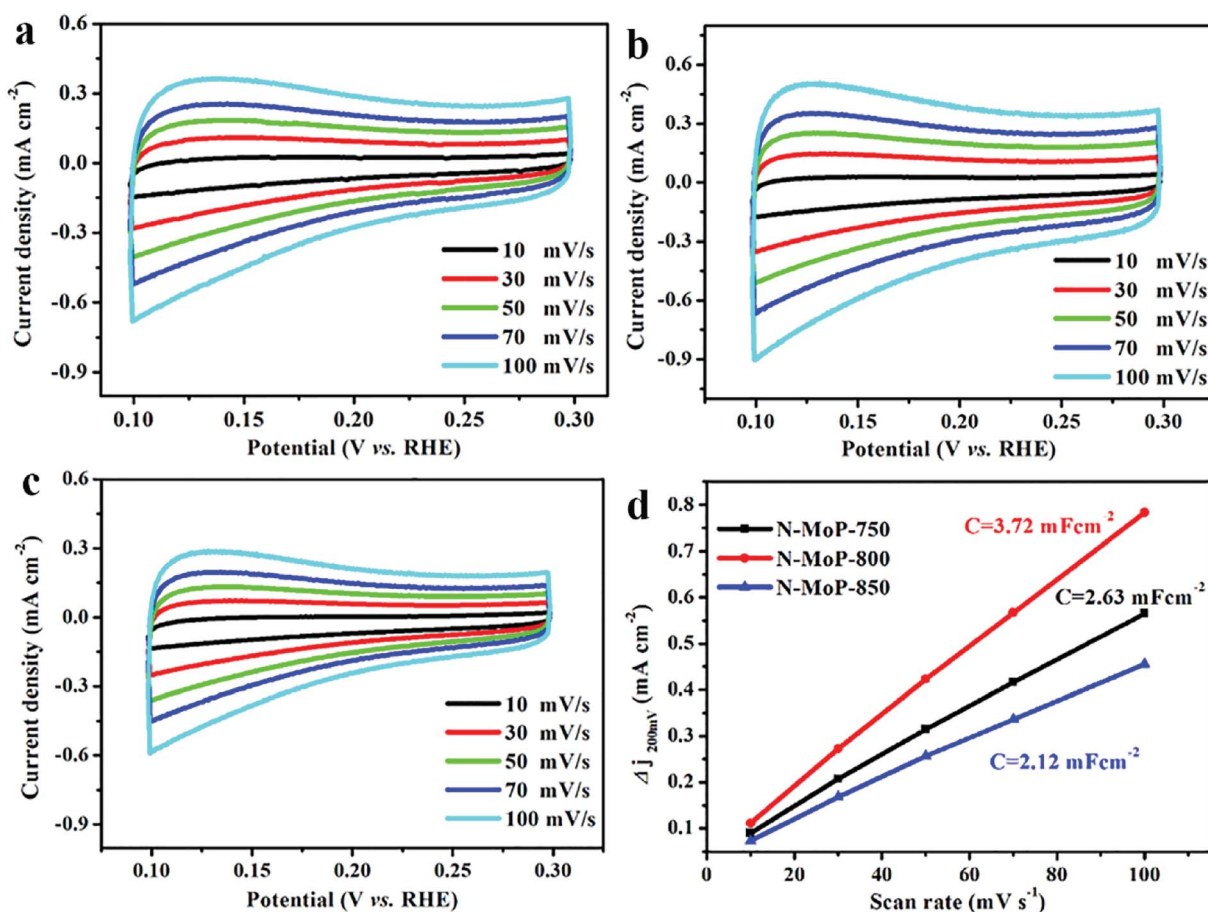


Fig. 4 CV curves for (a) N-MoP-750; (b) N-MoP-800 and (c) N-MoP-850 at different rates from 10 to 100  $\text{mV s}^{-1}$  in 0.5 M  $\text{H}_2\text{SO}_4$ ; (d) the relationship curve between capacitive current and scan rate for N-MoP-750, N-MoP-800 and N-MoP-850 at 0.2 V ( $\Delta j = j_a - j_c$ ).





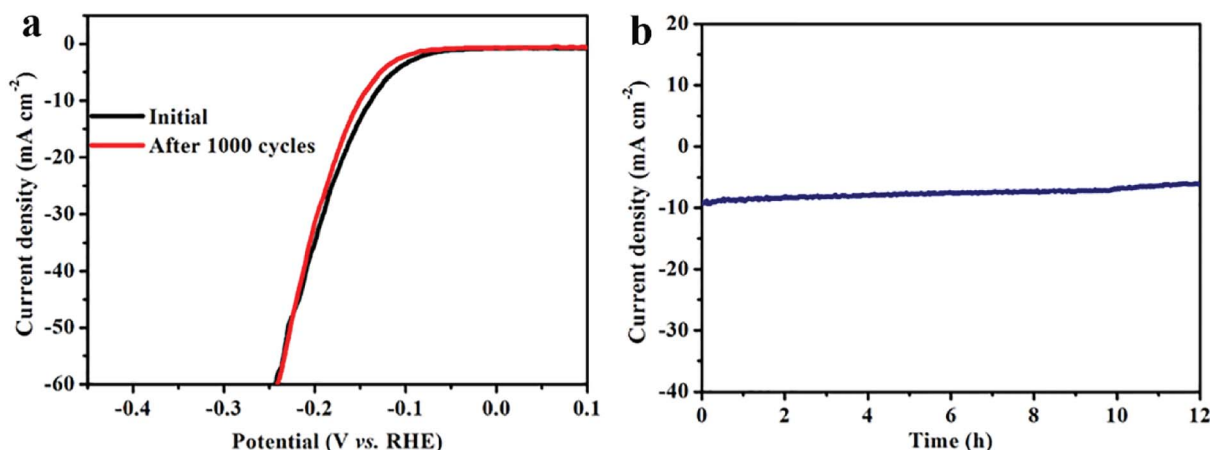


Fig. 5 (a) The polarization curves of N-MoP-800 before and after 1000 cycle testing; (b) the relationship plot of time dependence of current density for N-MoP-800 at a static overpotential of  $-142$  mV for 12 h in  $0.5$  M  $\text{H}_2\text{SO}_4$ .

results show that the N-MoP-750 has relatively high catalytic activity for HER in alkaline media. One suggests that high catalytic activity of N-MoP-750 may be associated with high proportion N-Mo component at sample surface. The formed N-

Mo component can optimal adsorption  $\text{OH}^-$  and hence exposure more active sites to boost HER performance in alkaline medium.<sup>58</sup> Fig. 6b shows the Tafel slopes for Pt/C, MoP, N-MoP-750, N-MoP-800, and N-MoP-850 are about 58.41, 132.69, 71.15,

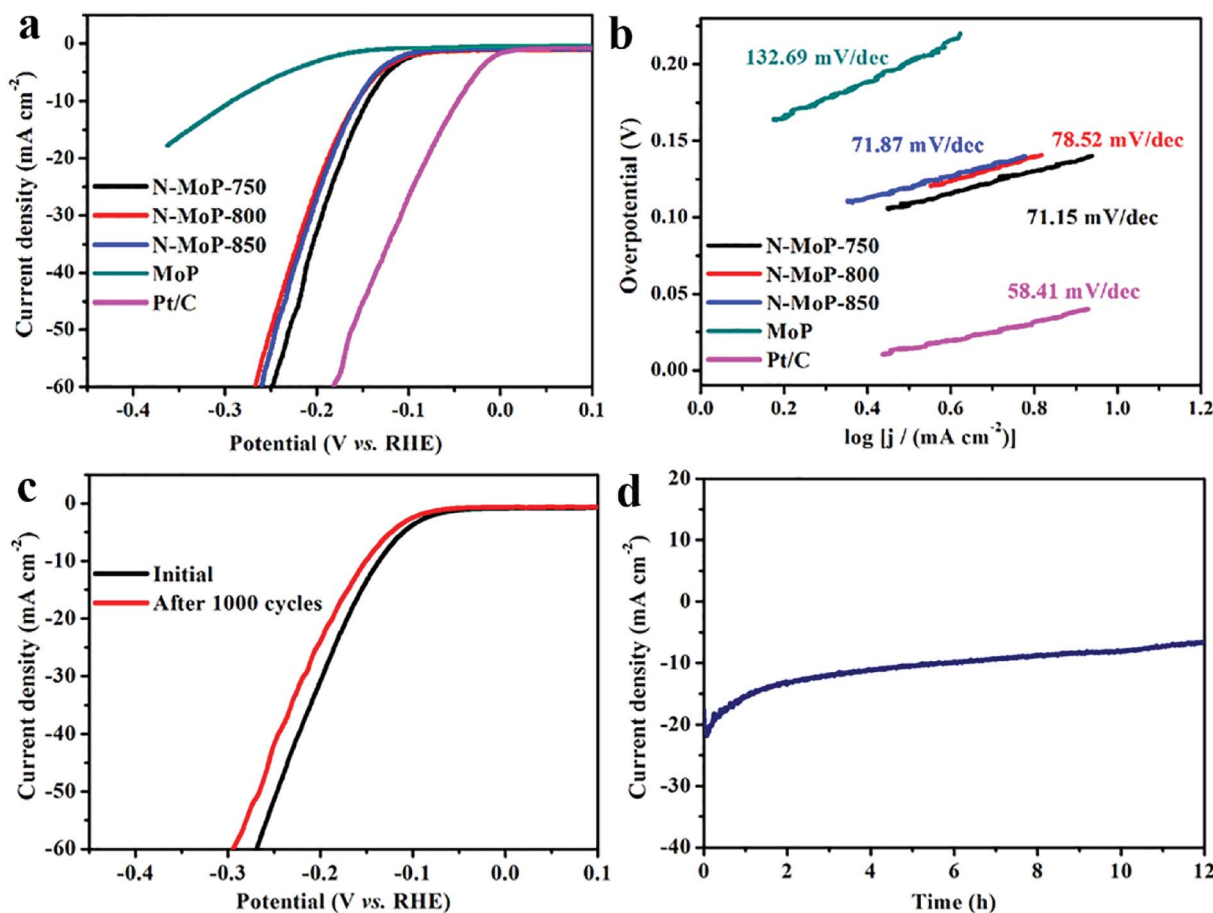


Fig. 6 HER performance of the prepared MoP-based materials in  $1$  M  $\text{KOH}$ , (a) polarization curves; (b) Tafel plots for MoP, N-MoP-750, N-MoP-800, N-MoP-850 and Pt/C; (c) the polarization curves of N-MoP-750 before and after 1000 cycles. (d) The time dependence of the current density for N-MoP-750 at a static overpotential of  $-154$  mV for 12 h.



78.52 and 71.87 mV dec<sup>-1</sup>, respectively, which suggests that the Volmer–Heyrovsky mechanism also takes effect on the HER process. To assess the durability of N-MoP-750, accelerated linear potential sweeps were conducted repeatedly on the electrodes. As shown in Fig. 6c, N-MoP-750 exhibits a continuous but small loss of activity before and after 1000 CV cycles, which implies minor corrosion of catalyst in alkaline condition. In addition, it was seen that current density of N-MoP-750 do not take obviously decaying during 12 h cyclic testing, implying high stability of N-MoP-750 (Fig. 6d). Taken together, the enhancement of HER performance of N-MoP-750 in alkaline medium can be ascribed to the two main factors: (i) the formation of high proportion Mo-N (49.87%) component on the surface can provide more active sites in alkaline medium that enhance catalytic dynamics for HER and favor their structural stability; (ii) the humps and edges on the surface of N-MoP-750 can contribute high active areas (ECSA ~ 62.3 cm<sup>2</sup>) and further accelerate electron transfer (Fig. S8†), which are responsible for the enhanced HER performance in alkaline solution. For comparison, the catalytic activity in HER of the as-prepared N-MoP nanorod and previously reported MoP-based electrocatalysts are listed in Table S1.† From Table S1,† it was seen that the HER performances of N-MoP are totally higher than most reported results. Based on the above analysis and discussions, it was concluded that desirable design of surface defects (N-doping) and humps on the surface play a key role in enhancing HER performances of N-MoP in both acidic and alkaline medium.

## 4. Conclusions

In summary, we reported a 1D porous N-MoP nanorod structure synthesized through a facile solution reaction, following by a calcination process. The prepared N-MoP exhibited high HER catalytic activities and good stability over a wide pH range. The high HER performance of N-MoP were attributed to the high electrical conductivity, more active sites caused by the N-doping and surface architectures. Our research proves that the N-MoP is a potential candidate for HER and provide a novel, eco-friendly and low-cost method to synthesize other 1D phosphides catalysts.

## Conflicts of interest

There are no conflicts to declare.

## Acknowledgements

We acknowledge funding support from the National Science Foundation of China (NSFC, No. 217031707), the State Key Laboratory of Solidification Processing in NWPU (No. SKLSP201613, and SKLSP201845).

## References

- 1 V. S. Thoi, Y. J. Sun, J. R. Long and C. J. Chang, *Chem. Soc. Rev.*, 2013, **42**, 2388–2400.

- 2 Y. Q. Qu and X. F. Duan, *Chem. Soc. Rev.*, 2013, **42**, 2568–2580.
- 3 M. S. Faber and S. Jin, *Energy Environ. Sci.*, 2014, **7**, 3519–3542.
- 4 C. G. Morales-Guio, L. A. Stern and X. L. Hu, *Chem. Soc. Rev.*, 2014, **43**, 6555–6569.
- 5 J. A. Turner, *Science*, 2004, **305**, 972–974.
- 6 A. J. Esswein and D. G. Nocera, *Chem. Rev.*, 2007, **107**, 4022–4047.
- 7 A. Kudo and Y. Miseki, *Chem. Soc. Rev.*, 2009, **38**, 253–278.
- 8 M. G. Walter, E. L. Warren, J. R. McKone, S. W. Boettcher, Q. X. Mi, E. A. Santori and N. S. Lewis, *Chem. Rev.*, 2010, **110**, 6446–6473.
- 9 D. Merki and X. L. Hu, *Energy Environ. Sci.*, 2011, **4**, 3878–3888.
- 10 D. Voiry, H. Yamaguchi, J. W. Li, R. Silva, D. C. B. Alves, T. Fujita, M. W. Chen, T. Asefa, V. B. Shenoy, G. Eda and M. Chhowalla, *Nat. Mater.*, 2013, **12**, 850–855.
- 11 S. Mandegarzar, J. B. Raoof, S. R. Hosseini and R. Ojani, *Electrochim. Acta*, 2016, **190**, 729–736.
- 12 D. Y. Wang, M. Gong, H. L. Chou, C. J. Pan, H. A. Chen, Y. P. Wu, M. C. Lin, M. Y. Guan, J. Yang, C. W. Chen, Y. L. Wang, B. J. Hwang, C. C. Chen and H. J. Dai, *J. Am. Chem. Soc.*, 2015, **137**, 1587–1592.
- 13 T. Wu, M. L. Stone, M. J. Shearer, M. J. Stolt, I. A. Guzei, R. J. Hamers, R. F. Lu, K. M. Deng, S. Jin and J. R. Schmidt, *ACS Catal.*, 2018, **8**, 1143–1152.
- 14 S. Tian, X. Li, A. J. Wang, R. Prins, Y. Y. Chen and Y. K. Hu, *Angew. Chem., Int. Ed.*, 2016, **55**, 4030–4034.
- 15 J. Q. Yan, H. Wu, P. Li, H. Chen, R. B. Jiang and S. Z. Liu, *J. Mater. Chem. A*, 2017, **5**, 10173–10181.
- 16 M. J. Liu, L. M. Yang, T. Liu, Y. H. Tang, S. L. Luo, C. B. Liu and Y. X. Zeng, *J. Mater. Chem. A*, 2017, **5**, 8608–8615.
- 17 X. Liang, D. Z. Zhang, Z. Z. Wu and D. Z. Wang, *Appl. Catal., A*, 2016, **524**, 134–138.
- 18 J. Q. Chi, W. K. Gao, J. H. Lin, B. Dong, K. L. Yan, J. F. Qin, Z. Z. Liu, Y. M. Chai and C. G. Liu, *J. Colloid Interface Sci.*, 2018, **513**, 151–160.
- 19 M. Cabán-Acevedo, M. L. Stone, J. R. Schmidt, J. G. Thomas, Q. Ding, H. C. Chang, M. L. Tsai, J. H. He and S. Jin, *Nat. Mater.*, 2015, **14**, 1245–1251.
- 20 X. Guo, G. L. Cao, F. Ding, X. Y. Li, S. Y. Zhen, Y. F. Xue, Y. M. Yan, T. Liu and K. N. Sun, *J. Mater. Chem. A*, 2015, **3**, 5041–5046.
- 21 Z. H. Pu, S. Y. Wei, Z. B. Chen and S. C. Mu, *RSC Adv.*, 2016, **6**, 11077–11080.
- 22 F. X. Ma, H. B. Wu, B. Y. Xia, C. Y. Xu and X. W. Lou, *Angew. Chem., Int. Ed.*, 2015, **54**, 15395–15399.
- 23 L. Liao, S. N. Wang, J. J. Xiao, X. J. Bian, Y. H. Zhang, M. D. Scanlon, X. L. Hu, Y. Tang, B. H. Liu and H. H. Girault, *Energy Environ. Sci.*, 2014, **7**, 387–392.
- 24 J. F. Xie, S. Li, X. D. Zhang, J. J. Zhang, R. X. Wang, H. Zhang, B. C. Pan and Y. Xie, *Chem. Sci.*, 2014, **5**, 4615–4620.
- 25 B. Qu, X. B. Yu, Y. J. Chen, C. L. Zhu, C. Y. Li, Z. X. Yin and X. T. Zhang, *ACS Appl. Mater. Interfaces*, 2015, **7**, 14170–14175.





- 26 H. Park, A. Encinas, J. P. Scheifers, Y. M. Zhang and B. P. T. Fokwa, *Angew. Chem., Int. Ed.*, 2017, **56**, 5575–5578.
- 27 J. Zhang, T. Wang, P. Liu, Z. Q. Liao, S. H. Liu, X. D. Zhuang, M. W. Chen, E. Zschech and X. L. Feng, *Nat. Commun.*, 2017, **8**, 15437.
- 28 W. X. Zhu, C. Tang, D. N. Liu, J. L. Wang, A. M. Asiric and X. P. Sun, *J. Mater. Chem. A*, 2016, **4**, 7169–7173.
- 29 G. Zhang, G. C. Wang, Y. Liu, H. J. Liu, J. H. Qu and J. H. Li, *J. Am. Chem. Soc.*, 2016, **138**, 14686–14693.
- 30 L. N. Zhang, S. H. Li, H. Q. Tan, S. U. Khan, Y. Y. Ma, H. Y. Zang, Y. H. Wang and Y. G. Li, *ACS Appl. Mater. Interfaces*, 2017, **9**, 16270–16279.
- 31 Z. X. Wu, J. W. J. Zhu, J. P. Guo, W. P. Xiao, C. J. Xuan, W. Lei and D. L. Wang, *Electrochim. Acta*, 2017, **232**, 254–261.
- 32 J. Yang, F. J. Zhang, X. Wang, D. S. He, G. Wu, Q. H. Yang, X. Hong, Y. Wu and Y. D. Li, *Angew. Chem., Int. Ed.*, 2016, **128**, 13046–13050.
- 33 A. K. Sun, Y. L. Shen, Z. Z. Wu and D. Z. Wang, *Int. J. Hydrogen Energy*, 2017, **42**, 14566–14571.
- 34 Q. W. Zhou, Z. H. Shen, C. Zhu, J. C. Li, Z. Y. Ding, P. Wang, F. Pan, Z. Y. Zhang, H. X. Ma, S. Y. Wang and H. G. Zhang, *Adv. Mater.*, 2018, 1800140.
- 35 T. R. Kuo, W. T. Chen, H. J. Liao, Y. H. Yang, H. C. Yen, T. W. Liao, C. Y. Wen, Y. C. Lee, C. C. Chen and D. Y. Wang, *Small*, 2017, **13**, 1603356.
- 36 T. Ling, D. Y. Yan, Y. Jiao, H. Wang, Y. Zheng, X. L. Zheng, J. Mao, X. W. Du, Z. P. Hu, M. Jaroniec and S. Z. Qiao, *Nat. Commun.*, 2016, **7**, 12876.
- 37 J. Yin, Y. J. Qiu, J. Yu, X. S. Zhou and W. H. Wu, *RSC Adv.*, 2013, **3**, 15655–15663.
- 38 J. Q. Chi, K. L. Yan, W. K. Gao, B. Dong, X. Shang, Y. R. Liu, X. Li, Y. M. Chai and C. G. Liu, *J. Alloys Compd.*, 2017, **714**, 26–34.
- 39 R. C. Li, L. J. Yang, T. L. Xiong, Y. S. Wu, L. D. Cao, D. S. Yuan and W. J. Zhou, *J. Power Sources*, 2017, **356**, 133–139.
- 40 Y. Zhao, S. Wang, C. Y. Li, X. B. Yu, C. L. Zhu, X. T. Zhang and Y. J. Chen, *RSC Adv.*, 2016, **6**, 7370–7377.
- 41 Q. S. Gao, S. N. Wang, H. C. Fang, J. W. Weng, Y. H. Zhang, J. J. Mao and Y. Tang, *J. Mater. Chem.*, 2012, **22**, 4709–4715.
- 42 Y. Y. Chen, Y. Zhang, W. J. Jiang, X. Zhang, Z. H. Dai, L. J. Wan and J. S. Hu, *ACS Nano*, 2016, **10**, 8851–8860.
- 43 Z. H. Pu, I. S. Amiin, X. B. Liu, M. Wang and S. C. Mu, *Nanoscale*, 2016, **8**, 17256–17261.
- 44 A. P. Wu, C. G. Tian, H. J. Yan, Y. Q. Jiao, Q. Yan, G. Y. Yang and H. G. Fu, *Nanoscale*, 2016, **8**, 11052–11059.
- 45 Z. H. Pu, S. Y. Wei, Z. B. Chen and S. C. Mu, *Appl. Catal., B*, 2016, **196**, 193–198.
- 46 S. M. Yin, J. Y. Han, Y. J. Zou, T. H. Zhou and R. Xu, *Nanoscale*, 2016, **8**, 14438–14447.
- 47 C. Deng, J. Z. Xie, Y. F. Xue, M. He, X. T. Wei and Y. M. Yan, *RSC Adv.*, 2016, **6**, 68568–68573.
- 48 Q. D. Yue, Y. Y. Wan, Z. J. Sun, X. J. Wu, Y. P. Yuan and P. W. Du, *J. Mater. Chem. A*, 2015, **3**, 16941–16947.
- 49 P. Xiao, M. A. Sk, L. Thi, X. M. Ge, R. J. Lim, J. Y. Wang, K. H. Lima and X. Wang, *Energy Environ. Sci.*, 2014, **7**, 2624–2629.
- 50 D. Z. Wang, Y. L. Shen, X. Y. Zhang and Z. Z. Wu, *J. Mater. Sci.*, 2017, **52**, 3337–3343.
- 51 R. Jiang, J. H. Fan, L. Y. Hu, Y. P. Dou, X. H. Mao and D. H. Wang, *Electrochim. Acta*, 2018, **261**, 578–587.
- 52 J. Jia, T. L. Xiong, L. L. Zhao, F. L. Wang, H. Liu, R. Z. Hu, J. Zhou, W. J. Zhou and S. W. Chen, *ACS Nano*, 2017, **11**, 12509–12518.
- 53 J. G. N. Thomas, *Trans. Faraday Soc.*, 1961, **57**, 1603–1611.
- 54 J. Kibsgaard, T. F. Jaramillo and F. Besenbacher, *Nat. Chem.*, 2014, **6**, 248–253.
- 55 W. L. Li, B. Herkt, M. Seredych and T. J. Bando, *Appl. Catal., B*, 2017, **207**, 195–206.
- 56 M. Sun, X. B. Wu, Z. Y. Xie, X. T. Deng, J. Y. Wen, Q. Z. Huang and B. Y. Huang, *Carbon*, 2017, **125**, 401–408.
- 57 L. J. Li, P. C. Dai, X. Gu, Y. Wang, L. T. Yan and X. B. Zhao, *J. Mater. Chem. A*, 2017, **5**, 789–795.
- 58 I. S. Amiin, Z. H. Pu, X. B. Liu, K. A. Owusu, H. G. R. Monestel, F. O. Boakye, H. N. Zhang and S. C. Mu, *Adv. Funct. Mater.*, 2017, **27**, 1702300.

